

Quantum Monte Carlo study of the Ne atom and the Ne^+ ion

N. D. Drummond, P. López Ríos, A. Ma, J. R. Trail,

G. Spink, M. D. Towler, and R. J. Needs

Theory of Condensed Matter Group, Cavendish Laboratory, University of Cambridge,

J. J. Thomson Avenue, Cambridge CB3 0HE, United Kingdom

February 2, 2008

Abstract

We report all-electron and pseudopotential calculations of the ground-state energies of the neutral Ne atom and the Ne^+ ion using the variational and diffusion quantum Monte Carlo (VMC and DMC) methods. We investigate different levels of Slater-Jastrow trial wave function: (i) using Hartree-Fock orbitals, (ii) using orbitals optimized within a Monte Carlo procedure in the presence of a Jastrow factor, and (iii) including backflow correlations in the wave function. Small reductions in the total energy are obtained by optimizing the orbitals, while more significant reductions are obtained by incorporating backflow correlations. We study the finite-time-step and fixed-node biases in the DMC energy, and show that there is a strong tendency for these errors to cancel when the first ionization potential (IP) is calculated. DMC gives highly accurate values for the IP of Ne at all the levels of trial wave function that we have considered.

1 Introduction

Accurate approximations to the many-electron wave function are required as inputs for the variational and diffusion quantum Monte Carlo (VMC and DMC) electronic-structure methods [1]. The quality of these “trial” wave functions determines both the statistical efficiency of the methods and the final accuracy that can be obtained, and one of the main technical challenges in the field of quantum Monte Carlo (QMC) simulation is to develop more accurate trial wave functions.

We report a detailed VMC and DMC study of the ground states of the Ne atom and the Ne^+ ion, in which several different forms of trial wave function have been used, and both all-electron and pseudopotential calculations have been performed. The difference between the ground-state energies of the neutral atom and the positive ion gives the first ionization potential (IP), which is known accurately from experiments [2]. The IP’s calculated using different wave functions are compared with the essentially exact nonrelativistic IP [3] and the experimental value. We also demonstrate the degree to which the DMC fixed-node and time-step errors cancel when the IP is calculated.

The basic form of wave function that we study consists of a product of Slater determinants for spin-up and spin-down electrons containing Hartree-Fock (HF) orbitals, multiplied by a positive Jastrow correlation factor. We consider the effects of optimizing the orbitals in the presence of the Jastrow factor [4, 5], and the effects of including backflow correlations in the wave function [6, 7, 8]. We have also carried out some tests using multideterminant wave functions [9, 10], but we were not able to lower the DMC energy using this approach.

The rest of this paper is organized as follows. In Sec. 2 we briefly review the VMC and DMC methods, while in Sec. 3 we describe the different levels of Slater-Jastrow wave function that we investigate. In Sec. 4 we study time-step bias in DMC calculations of the total energy and IP of Ne. The total energies and IP’s calculated using different trial wave functions are compared in Sec. 5. Finally, we draw our conclusions in Sec. 6.

We use Hartree atomic units, $\hbar = |e| = m_e = 4\pi\epsilon_0 = 1$, throughout. All of our QMC calculations were performed using the CASINO code [11].

2 QMC methods

The VMC energy is calculated as the expectation value of the Hamiltonian operator with respect to a trial wave function, the integrals being performed by a Monte Carlo method. In DMC, the imaginary-time Schrödinger equation is used to evolve a set of configurations towards the ground-state distribution. Fermionic symmetry is maintained by the fixed-node approximation [12], in which the nodal surface of the wave function is constrained to equal that of a trial wave function. Our DMC algorithm is essentially that of Umrigar *et al.* [13]. Various modifications to the DMC Green's function were proposed by Umrigar *et al.* to reduce the time-step errors in all-electron calculations, and we investigate the effects of these modifications in Sec. 4.

For most of our pseudopotential calculations we used a nonrelativistic HF Ne pseudopotential (effective core potential), although for our investigations of time-step errors we used a Dirac-Fock averaged-relativistic effective potential (AREP) [14, 15]. These pseudopotentials are finite at the origin, making them particularly suitable for use in QMC calculations. There is evidence [16] that neglecting correlation effects entirely when constructing pseudopotentials, as in HF and Dirac-Fock theory, provides better pseudopotentials for use in correlated valence calculations than density-functional-theory-derived pseudopotentials. Part of the motivation for performing the calculations reported here is to test the Ne pseudopotentials in correlated valence calculations. The contributions to the total energy from the nonlocal components of the pseudopotential within DMC were calculated using the locality approximation [17], which leads to errors that are second order in the error in the trial wave function [18].

3 Trial wave functions

3.1 Basic Slater-Jastrow wave function with HF orbitals

The Slater-Jastrow wave function may be written as

$$\Psi(\mathbf{R}) = \exp[J(\mathbf{R})] \sum_i \mu_i D_i^\uparrow(\mathbf{R}) D_i^\downarrow(\mathbf{R}), \quad (1)$$

where $\mathbf{R} \equiv (\mathbf{r}_1, \dots, \mathbf{r}_N)$ denotes the spatial coordinates of all the electrons, $\exp[J(\mathbf{R})]$ is the Jastrow correlation factor, $D_i^\uparrow(\mathbf{R})$ and $D_i^\downarrow(\mathbf{R})$ are Slater determinants of orbitals for spin-up and spin-down electrons, and the $\{\mu_i\}$ are expansion coefficients. The Jastrow factor, which describes the dynamic correlation of the electrons, is an explicit function of the interparticle distances. We use the form of Jastrow factor described in Ref. [19]. In our calculations the Slater determinants $\{D_i^\sigma\}$ were formed from single-particle orbitals obtained from restricted open-shell HF calculations using numerical integration on radial grids. The all-electron HF calculations were performed using the code of Fischer [20] and the pseudopotential HF calculations were performed using our own code. The variable parameters in the trial wave functions were determined by minimizing the unweighted variance of the energy [4, 21, 22].

We also performed tests using multideterminant trial wave functions. The determinants were obtained from multiconfiguration HF calculations performed by numerical integration on radial grids, the expansion coefficients $[\{\mu_i\}$ in Eq. (1)] being re-optimized in the presence of the Jastrow factor using unweighted variance minimization [22]. During the optimization process, we constrained the coefficients of the determinants within each configuration state function to have the same magnitude, so that the symmetry of the wave function was maintained. We were able to achieve significantly lower VMC energies than we could with the single-determinant Slater-Jastrow wave function, but the DMC energies were higher than the single-determinant ones. All numerical results reported in this article were obtained with a single term in the determinant expansion.

3.2 Modification of the HF orbitals

Altering parameters in the orbitals moves the nodal surface of the trial wave function and therefore changes the value of the fixed-node DMC energy. This is not the case for parameters in the Jastrow factor. Optimizing the orbitals in the presence of a Jastrow factor generally improves the nodal surface of the wave function and therefore lowers the DMC energy, which satisfies a variational principle with respect to errors in the nodal surface [23, 24]. Unfortunately, optimizing parameters that affect the nodal surface by unweighted variance minimization is problematic. At each iteration, a minimization is performed using a fixed set of sampling points in the configuration space, and the nodal surface deforms continuously as the parameter

values are altered. In the course of this deformation, the nodal surface may pass through one of the fixed configurations, at which point the estimate of the unweighted variance of the local energy ($\Psi^{-1}\hat{H}\Psi$, where \hat{H} is the Hamiltonian operator) diverges. This makes it difficult to locate the true minimum of the unweighted variance. It is possible to improve the situation by using the weight-limiting scheme described in Ref. [22], which effectively removes configurations whose local energies are diverging from the set used to calculate the variance. Alternatively, the reweighted variance-minimization algorithm can be used, where each configuration is weighted by the ratio of the square of the current wave function to the probability density according to which the configurations were distributed, so that the calculated variance is an estimate of the actual variance of the energy. Reweighted variance minimization does not suffer from the problem of divergences in the variance but, nevertheless, the unweighted algorithm gives significantly lower variational energies in practice, and we used this method for all the optimizations reported here. However, the difficulty in locating the global minimum of the variance with respect to parameters that affect the nodal surface makes it more difficult to optimize the orbitals for two different systems to the same level of accuracy.

The atomic orbitals that we have used can be expressed in the form

$$\psi_{nlm}(\mathbf{r}) = [\rho_{nl}^{\text{HF}}(r) + \Delta\rho_{nl}(r)] r^l Y_{lm}(\theta, \phi), \quad (2)$$

where we have used spherical polar coordinates, with r , θ , and ϕ being the radial, polar, and azimuthal coordinates of the point \mathbf{r} . The origin is chosen to lie at the nucleus. $Y_{lm}(\theta, \phi)$ is the (l, m) th spherical harmonic, and $\rho_{nl}^{\text{HF}}(r)$ is the HF radial function. (Note that, in practice, we use appropriate linear combinations of spherical harmonics with a given l in order to construct real orbitals.) The modification to the HF radial function is written as

$$\Delta\rho_{nl}(r) = \left(\sum_{j=0}^N c_{jnl} r^j \right) \exp\left(\frac{-A_{nl}r^2}{1 + B_{nl}r} \right), \quad (3)$$

where A_{nl} , B_{nl} and $\{c_{0nl}, \dots, c_{Nnl}\}$ are optimizable parameters. Obviously we must have $A_{nl} > 0$ and $B_{nl} \geq 0$, otherwise the orbital will be non-normalizable. The chosen form of the modification to the radial function has considerable variational freedom and decays exponentially at large distances. The HF orbitals minimize the energy in the absence of a Jastrow factor, although they are no longer optimal when a Jastrow factor is included; however we expect $\Delta\rho_{nl}(r)$ to remain small in this case. After some experimentation we decided to use $N = 3$ for the all-electron calculations and $N = 6$ for the pseudopotential ones, as these

choices allowed us to achieve the lowest variational energies in our tests.

Kato derived a condition on the spherical average of the wave function about a bare nucleus of atomic number Z at the origin [25]:

$$\left(\frac{\partial\langle\Psi\rangle}{\partial r_i}\right)_{r_i=0} = -Z\langle\Psi\rangle_{r_i=0}, \quad (4)$$

where $r_i = |\mathbf{r}_i|$ and $\langle\Psi\rangle$ is the spherical average of the many-body wave function about $r_i = 0$. If the wave function is nonzero at the nucleus (as is the case for the ground-state wave functions studied in the present work), then it is possible to carry out accurate and stable QMC calculations if and only if the Kato cusp condition [Eq. (4)] is satisfied [1]. It is easy to show that a Slater-Jastrow wave function obeys the electron-nucleus Kato cusp condition if each orbital satisfies Eq. (4) individually and the Jastrow factor is cusplless at the nucleus. (It is preferable to impose the electron-nucleus cusp condition via the orbitals rather than the Jastrow factor [19].) The spherical averages of orbitals with $l \neq 0$ are zero, and therefore these orbitals obey the Kato cusp condition automatically, but we must impose Eq. (4) on the radial parts of the s orbitals. This gives us the requirement that $c_{1n0} = -Zc_{0n0}$, where Z is the atomic number of the atom in an all-electron calculation and $Z = 0$ for a calculation using a pseudopotential which is finite at the nucleus.

3.3 Backflow correlations

We have also investigated the effect of incorporating backflow correlations in the trial wave function. Classical backflow is related to the flow of a fluid around a large impurity, and its quantum analog was first discussed by Feynman [6] and Feynman and Cohen [7] in the contexts of excitations in ^4He and the effective mass of a ^3He impurity in liquid ^4He . Backflow correlations have previously been used in trial wave functions for fermion QMC simulations of two-dimensional [8] and three-dimensional [26] electron gases, and metallic hydrogen [27]. The original derivation of backflow correlations by Feynman [6] was based on the idea of local current conservation, although they can also be derived from an imaginary-time evolution argument [8, 28].

The backflow correlations are described by replacing the electron coordinates $\{\mathbf{r}_i\}$ in the Slater determinants of Eq. (1) by “quasiparticle” coordinates $\{\mathbf{x}_i\}$, defined to be

$$\mathbf{x}_i = \mathbf{r}_i + \sum_{j \neq i} [F(r_{ij}, r_i, r_j)(\mathbf{r}_i - \mathbf{r}_j) + G(r_{ij}, r_i, r_j)\mathbf{r}_j], \quad (5)$$

where F and G are functions that contain parameters to be determined by variance minimization, and $r_{ij} = |\mathbf{r}_i - \mathbf{r}_j|$. In our work, $F(r_{ij}, r_i, r_j)$ and $G(r_{ij}, r_i, r_j)$ consist of smoothly truncated polynomial expansions in r_i , r_j , and r_{ij} , of the same form as the isotropic terms that occur in the Jastrow factor introduced in Ref. [19].

In our all-electron calculations the electron-nucleus cusp conditions are enforced via the orbitals in the Slater determinants, and in order to preserve the cusp conditions when backflow is included we ensure that F and G go smoothly to zero as an electron approaches the nucleus. We use pseudopotentials that are smooth at the nucleus and we therefore choose G to be smooth at the nucleus in our pseudopotential calculations. The electron-electron Kato cusp conditions are enforced by the Jastrow factor in our calculations, and the backflow functions are chosen to preserve these conditions. Our implementation of backflow correlations for systems containing many atoms will be described elsewhere [29].

4 Investigations of time-step errors

We have studied the time-step bias in all-electron and Dirac-Fock AREP pseudopotential DMC calculations of the ground-state energies of the Ne atom and the Ne^+ ion [14, 15]. Figures 1 and 2 show the DMC energy obtained at different time steps, both with and without the modifications to the all-electron DMC Green's function proposed in Ref. [13]. The all-electron energies enter the small-time-step regime (where the bias in the DMC energy is nearly linear in the time step) at time steps less than about 0.005 a.u. The root-mean-square distance diffused at each time step of 0.005 a.u. is about 0.12 a.u., which is close to the Bohr radius of Ne ($1/Z = 0.1$ a.u.); this is the length scale relevant to the core ($1s$) electrons, suggesting that they are responsible for much of the time-step bias. The time-step bias remains small up to much larger time steps in the pseudopotential calculations, again implying that the $1s$ electrons are responsible for most of the bias in the all-electron results. The contribution to the time-step bias from the core region is expected to be large, because the energy scale of the innermost electrons is greater than the energy scale of the outer electrons, although this is offset by the fact that the wave function is relatively accurate in the vicinity of the nucleus.

It is clear from Figs. 1 and 2 that the modifications to the all-electron DMC Green's function successfully

eliminate much of the time-step bias due to the innermost electrons at small time steps. On the other hand, the form of the time-step bias is almost the same for the Ne atom and the Ne^+ ion, suggesting that the bias will cancel out when the IP is calculated, irrespective of whether the Green's function modifications are used. It can be seen in Fig. 3, which shows the IP as a function of time step, that this is indeed the case. Since the bias is largely caused by the innermost electrons, which are in almost identical environments in Ne and Ne^+ , this strong cancellation is to be expected.

If a basic Slater-Jastrow wave function is used then the zero-time-step limit of the DMC energy is determined by the nodes of the HF wave function, independent of the Jastrow factor, whereas the DMC energy at finite time steps does depend on the Jastrow factor. However, provided that similar levels of Jastrow factor are used for systems to be compared (with the core electrons in the same configuration), it is reasonable to expect a large degree of cancellation of bias to occur when energy differences are taken at finite time steps.

5 Energies of Ne and Ne^+

In Table 1 we present values for the total nonrelativistic energies of Ne and Ne^+ and the nonrelativistic IP of Ne, calculated using a number of different electronic-structure methods. For the all-electron atom and ion, we give results obtained using HF theory (AHF), density-functional theory using the local spin-density approximation (DFT-LSDA), Perdew-Wang (DFT-PW91), and Becke-Lee-Yang-Parr (DFT-BLYP) exchange-correlation functionals, all-electron VMC and DMC using a basic Slater-Jastrow wave function with HF orbitals (AVMC and ADMC), all-electron VMC and DMC using a Slater-Jastrow wave function with optimized orbitals (AOVMC and AODMC), all-electron VMC and DMC with HF orbitals and backflow correlations (ABVMC and ABDMC), and all-electron VMC and DMC with optimized orbitals and backflow correlations (AOBVMC and AOBDMC). For the pseudopotential calculations, which used a nonrelativistic HF pseudopotential [14, 15], we give results obtained using HF theory (PHF), VMC and DMC using a basic Slater-Jastrow wave function with HF orbitals (PVMC and PDMC), VMC and DMC using a Slater-Jastrow wave function with optimized orbitals (POVMC and PODMC), VMC and DMC with HF orbitals and backflow correlations (PBVMC and PBDMC), and VMC and DMC with optimized orbitals and backflow

correlations (POBVMC and POBDMC). For each of the VMC calculations we give the total number of parameters in the trial wave function that were optimized using unreweighted variance minimization, along with the expectation value of the variance of the energy. Furthermore, we give the fraction of the correlation energy retrieved by the wave function. In the all-electron calculations, the correlation energy is defined to be the difference between the HF energy and the exact nonrelativistic energy. In the pseudo-Ne calculations, the correlation energy is defined to be the difference between the HF energy and the PBDMC energy. The DFT-LSDA IP is taken from Ref. [30], while the DFT-PW91 and DFT-BLYP results are taken from Ref. [31]. The “exact” nonrelativistic (NR) infinite-nuclear-mass energies are taken from Ref. [3].

All the DMC energies quoted in Table 1 have been extrapolated to zero time step. We used a range of small time steps and performed linear extrapolations of the energies to zero time step.

Optimizing the orbitals reduces the VMC energy, but does not have a significant effect on the DMC energy, except in the case of the pseudopotential calculation with backflow correlations, where optimizing the orbitals actually increases the DMC energy, presumably because the very large number of variable parameters adversely affects the optimization. The VMC variance is very slightly reduced by optimizing the orbitals in the all-electron calculations, but not in the pseudopotential calculations. (Note that, as discussed in Ref. [22], the unreweighted variance-minimization algorithm does not generally minimize the expected variance of the energy.) The inclusion of backflow correlations reduces the errors in the VMC energies by a factor of about 2, and reduces the variances of the VMC energies by a factor of between 2 and 3. For both pseudopotential and all-electron calculations, the percentage of the total correlation energy retrieved within VMC is slightly larger for Ne than for Ne^+ , although the difference is smaller in DMC.

The previous lowest VMC energy in the literature for the all-electron Ne atom is due to Huang *et al.* [32], who used a single-determinant trial wave function with optimized orbitals and Jastrow factor, corresponding to our AOVMC level of calculation, and obtained an energy of $-128.9029(3)$ a.u., which amounts to 91.11(8)% of the correlation energy. Our AOVMC energy of $-128.90334(9)$ a.u. (91.23(2)% of the correlation energy) is very similar. We obtain a VMC energy of $-128.9205(2)$ a.u. (95.62(5)% of the correlation energy) at the AOBVMC level, so that backflow retrieves about 50.1(7)% of the remaining correlation energy. Note also that the VMC energies obtained with backflow are very similar to the DMC energies without backflow, for

both the all-electron and pseudopotential calculations. This indicates that VMC with backflow may be a useful level of theory, because VMC calculations are significantly less costly than DMC ones, and VMC has advantages for calculating expectation values of quantities other than the energy.

At the DMC level backflow retrieves about 38(2)% of the correlation energy missing at the AODMC level. Our AOBDMC energy of $-128.9290(2)$ a.u. (97.80(5)% of the correlation energy) is significantly lower than the previous lowest DMC energy in the literature of $-128.9243(8)$ a.u. (96.6(2)% of the correlation energy) [32].

The increase in the complexity of the wave function resulting from the inclusion of backflow correlations is apparent from the three- to five-fold increase in the number of parameters in the wave function. However, the use of backflow or orbital optimization does not result in any clear improvement to the VMC or DMC IP's. The all-electron DMC IP's obtained with the different forms of wave function are very close to one another. The inclusion of backflow in the pseudopotential calculations results in a small increase in the IP (away from the experimental result). This may reflect the fact that it is harder to optimize a backflow function for Ne^+ , where the symmetry between up and down spins is broken, or it may be an indication of the error inherent in the pseudopotential approximation.

Irrespective of the form of trial wave function used, or whether all-electron or pseudopotential calculations are performed, or whether the VMC or DMC method is used, all of the QMC calculations give excellent values for the IP. In the worst cases the errors in the VMC nonrelativistic IP's are 0.43(4)% (all-electron) and 0.60(3)% (pseudopotential) and the errors in the DMC nonrelativistic IP's are 0.28(4)% (all-electron) and 0.35(4)% (pseudopotential). The considerably larger errors in the HF IP (8%) and DFT IP's (1.7% for the best case of the BLYP functional) demonstrate the importance of describing electron correlation accurately when calculating the IP.

The correction to the IP of Ne from the finite mass of the nucleus is of order 10^{-5} a.u., which is negligible on the scale of interest. The total relativistic correction to the IP of Ne has been estimated to be -0.00196 a.u. [3], which is significant on the scale of interest: see Fig. 3. Adding this correction to our best DMC data, obtained at the AOBDMC level, gives an IP of $0.7945(2)$ a.u., which is only $0.0020(2)$ a.u. (0.054(5) eV) larger than the experimental value of 0.792481 a.u. (21.5645 eV) [2]. Using the same relativistic correction for

the pseudopotential POBDMC data gives an IP which is 0.0026(3) a.u. (0.071(8) eV) larger than experiment. The error in the IP due to the use of the pseudopotential is therefore about 0.0006(4) a.u. (0.016(11) eV), which is less than 0.1% of the IP.

6 Conclusions

We have performed all-electron and pseudopotential VMC and DMC calculations of the total energies of Ne and Ne^+ using basic Slater-Jastrow wave functions with HF orbitals, Slater-Jastrow wave functions with optimized orbitals, and wave functions including backflow correlations. We have found that optimizing the orbitals makes a small improvement to the VMC energy, but has very little effect on the DMC energy. The HF orbitals give nearly optimal single-determinant nodal surfaces for the ground states of Ne and Ne^+ , although this cannot be expected to hold for other systems. On the other hand, including backflow correlations lowers both the VMC and DMC energies significantly, giving us the lowest VMC and DMC energies for all-electron Ne in the literature to date. However, the improvements in the total energies of Ne and Ne^+ hardly affect the calculated IP, because they almost exactly cancel when the energy difference is evaluated. Overall, the calculated IP's are slightly too large, because the wave functions for Ne^+ are not quite as accurate as those for Ne.

Including backflow correlations for Ne and Ne^+ reduced the error in the VMC total energy by a factor of about 2 and reduced the variance of the VMC energy by a factor of between 2 and 3. Reducing the variance improves the statistical efficiency of VMC calculations, while reducing the error in the VMC total energy improves the statistical efficiency of DMC calculations [33, 34]. The incorporation of backflow is expected to improve the QMC estimates of all expectation values, not just the energy. Including backflow correlations is costly, however, because every element in the Slater determinant has to be recomputed each time an electron is moved, whereas only a single column of the Slater determinant has to be updated after each move when the basic Slater-Jastrow wave function is used. In the case of Ne, including backflow correlations increased the computational cost per move in VMC and DMC by a factor of between 4 and 7. However, the reduction in the variance meant that the number of moves required to obtain a fixed error bar in the energy was smaller; hence, overall, including backflow correlations increased the time taken to perform the

calculations by a factor of between 2 and 3. Backflow functions introduce additional variable parameters into the trial wave function, making the optimization procedure more difficult and costly. Nodal surfaces obtained from HF or DFT orbitals do not suffer from statistical errors. By contrast, the parameters in the backflow functions are optimized by a Monte Carlo method, and therefore the nodal surface is subject to stochastic noise. Furthermore, although Jastrow factors are easy to optimize using unweighted variance minimization with a fixed distribution of configurations, parameters that affect the nodal surface are relatively difficult to optimize, because the local energy diverges at the nodes.

We have investigated the time-step bias in the DMC total energies of Ne and Ne^+ and the IP of Ne. The time-step errors in the pseudopotential calculations were relatively small, indicating that the bias in the all-electron total energy was mainly due to the $1s$ electrons. In IP calculations using a basic Slater-Jastrow wave function with HF orbitals the time-step bias largely canceled out when the difference of energies was taken, irrespective of whether the modifications to the all-electron DMC Green's function proposed in Ref. [13] were used. The time-step errors in the IP were considerably smaller in the pseudopotential calculations than the all-electron ones.

Most importantly, our results demonstrate the superb accuracy of the DMC method for this problem. After including a correction for relativistic effects, our all-electron IP of Ne is about 0.0020 a.u. (0.054 eV) larger than the experimental value [2] of 0.792481 a.u. (21.5645 eV). Our pseudopotential IP is about 0.0026 a.u. (0.071 eV) larger than the experimental value, demonstrating the accuracy of the pseudopotentials we use [14, 15].

7 Acknowledgments

Financial support has been provided by the Engineering and Physical Sciences Research Council of the United Kingdom. N.D.D. acknowledges financial support from Jesus College, Cambridge. P.L.R. gratefully acknowledges the financial support provided through the European Community's Human Potential Programme under contract HPRN-CT-2002-00298, RTN "Photon-Mediated Phenomena in Semiconductor Nanostructures." Computer resources have been provided by the Cambridge-Cranfield High Performance Computing Facility.

References

- [1] W. M. C. Foulkes, L. Mitas, R. J. Needs, and G. Rajagopal, *Rev. Mod. Phys.* **73**, 33 (2001).
- [2] V. Kaufman and L. Minnhagen, *J. Opt. Soc. Am.* **62**, 92 (1972).
- [3] S. J. Chakravorty, S. R. Gwaltney, E. R. Davidson, F. A. Parpia, and C. F. Fischer, *Phys. Rev. A* **47**, 3649 (1993).
- [4] C. J. Umrigar, K. G. Wilson, and J. W. Wilkins, *Phys. Rev. Lett.* **60**, 1719 (1988).
- [5] C. Filippi and S. Fahy, *J. Chem. Phys.* **112**, 3523 (2000).
- [6] R. P. Feynman, *Phys. Rev.* **94**, 262 (1954).
- [7] R. P. Feynman and M. Cohen, *Phys. Rev.* **102**, 1189 (1956).
- [8] Y. Kwon, D. M. Ceperley, and R. M. Martin, *Phys. Rev. B* **48**, 12037 (1993).
- [9] C. Filippi and C. J. Umrigar, *J. Chem. Phys.* **105**, 213 (1996).
- [10] F. Schautz and S. Fahy, *J. Chem. Phys.* **116**, 3533 (2002).
- [11] R. J. Needs, M. D. Towler, N. D. Drummond, and P. López Ríos, *CASINO version 2.0 User Manual*, University of Cambridge, Cambridge (2005).
- [12] J. B. Anderson, *J. Chem. Phys.* **65**, 4121 (1976).
- [13] C. J. Umrigar, M. P. Nightingale, and K. J. Runge, *J. Chem. Phys.* **99**, 2865 (1993).
- [14] J. R. Trail and R. J. Needs, *J. Chem. Phys.* **122**, 174109 (2005).
- [15] J. R. Trail and R. J. Needs, *J. Chem. Phys.* **122**, 014112 (2005).
- [16] C. W. Greeff and W. A. Lester, Jr., *J. Chem. Phys.* **109**, 1607 (1998).
- [17] M. M. Hurley and P. A. Christiansen, *J. Chem. Phys.* **86**, 1069 (1987).
- [18] L. Mitáš, E. L. Shirley, and D. M. Ceperley, *J. Chem. Phys.* **95**, 3467 (1991).

- [19] N. D. Drummond, M. D. Towler, and R. J. Needs, Phys. Rev. B **70**, 235119 (2004).
- [20] G. Gaigalas and C. F. Fischer, Comput. Phys. Commun. **98**, 255 (1996).
- [21] P. R. C. Kent, R. J. Needs, and G. Rajagopal, Phys. Rev. B **59**, 12344 (1999).
- [22] N. D. Drummond and R. J. Needs, Phys. Rev. B **72**, 085124 (2005).
- [23] P. J. Reynolds, D. M. Ceperley, B. J. Alder, and W. A. Lester, Jr., J. Chem. Phys. **77**, 5593 (1982).
- [24] W. M. C. Foulkes, R. Q. Hood, and R. J. Needs, Phys. Rev. B **60**, 4558 (1999).
- [25] T. Kato, Commun. Pure Appl. Math. **10**, 151 (1957).
- [26] Y. Kwon, D. M. Ceperley, and R. M. Martin, Phys. Rev. B **58**, 6800 (1998).
- [27] C. Pierleoni, D. M. Ceperley, and M. Holzmann, Phys. Rev. Lett. **93**, 146402 (2004).
- [28] M. Holzmann, D. M. Ceperley, C. Pierleoni, and K. Esler, Phys. Rev. E **68**, 046707 (2003).
- [29] P. López Ríos *et al.*, unpublished.
- [30] J. P. Perdew, J. A. Chevary, S. H. Vosko, K. A. Jackson, M. R. Pederson, D. J. Singh, and C. Fiolhais, Phys. Rev. B **46**, 6671 (1992).
- [31] T. Grabo, T. Kreibich, S. Kurth, and E. K. U. Gross, in *Strong Coulomb Correlations in Electronic Structure: Beyond the Local Density Approximation*, ed. V. I. Anisimov (Gordon and Breach, Tokyo, 1998).
- [32] C.-J. Huang, C. J. Umrigar, and M. P. Nightingale, J. Chem. Phys. **107**, 3007 (1997).
- [33] D. M. Ceperley, J. Stat. Phys. **43**, 815 (1986).
- [34] A. Ma, M. D. Towler, N. D. Drummond, and R. J. Needs, J. Chem. Phys. **122**, 224322 (2005).

Table

Meth.	No. param.		Energy (a.u.)		%age corr. en.		Variance (a.u.)		IP (a.u.)
	Ne	Ne ⁺	Ne	Ne ⁺	Ne	Ne ⁺	Ne	Ne ⁺	
Exact NR	–	–	–128.9376	–128.1431	100.0	100.0	–	–	0.7945
DFT-LSDA	–	–	–	–	–	–	–	–	0.812
DFT-PW91	–	–	–	–	–	–	–	–	0.812
DFT-BLYP	–	–	–	–	–	–	–	–	0.808
AHF	–	–	–128.54710	–127.81781	0.0	0.0	–	–	0.72928
AVMC	75	79	–128.8983(2)	–128.1016(1)	89.94(5)	87.24(3)	1.12(2)	1.047(1)	0.7967(2)
AOVMC	88	92	–128.90334(9)	–128.10760(6)	91.23(2)	89.09(2)	0.9740(9)	0.938(3)	0.79574(11)
ABVMC	205	209	–128.9190(2)	–128.1213(2)	95.24(5)	93.30(6)	0.421(1)	0.406(2)	0.7979(3)
AOBVMC	218	222	–128.9205(2)	–128.1240(2)	95.62(5)	94.13(6)	0.391(1)	0.379(3)	0.7965(3)
ADMC	–	–	–128.9233(2)	–128.1266(2)	96.34(5)	94.93(6)	–	–	0.7967(3)
AODMC	–	–	–128.9237(2)	–128.1273(2)	96.44(5)	95.14(6)	–	–	0.7964(3)
ABDMC	–	–	–128.9287(2)	–128.1321(1)	97.72(5)	96.62(3)	–	–	0.7966(2)
AOBDMC	–	–	–128.9290(2)	–128.1325(1)	97.80(5)	96.74(3)	–	–	0.7965(2)
PHF	–	–	–34.59111	–33.86129	0.0	0.0	–	–	0.72982
PVMC	53	61	–34.88930(4)	–34.09453(4)	93.10(6)	92.26(7)	0.3955(6)	0.3994(8)	0.79477(6)
POVMC	70	76	–34.88973(4)	–34.09472(4)	93.23(6)	92.33(7)	0.4024(7)	0.391(1)	0.79501(6)
PBVMC	275	291	–34.90509(6)	–34.1059(2)	98.03(6)	96.8(1)	0.1748(7)	0.226(2)	0.7992(2)
POBVMC	292	300	–34.90475(6)	–34.1055(2)	97.92(6)	96.6(1)	0.1483(7)	0.222(2)	0.7993(2)
PDMC	–	–	–34.9026(2)	–34.1072(2)	97.25(9)	97.3(1)	–	–	0.7954(3)
PODMC	–	–	–34.9028(2)	–34.1074(2)	97.31(9)	97.3(1)	–	–	0.7954(3)
PBDMC	–	–	–34.9114(2)	–34.1141(2)	100.00(9)	100.0(1)	–	–	0.7973(3)
POBDMC	–	–	–34.9099(2)	–34.1128(2)	99.53(9)	99.5(1)	–	–	0.7971(3)

Table 1: Numbers of parameters in trial wave functions, ground-state energies, percentages of correlation energies retrieved, energy variances, and IP’s of all-electron Ne (and Ne⁺) and pseudo-Ne (and pseudo-Ne⁺), obtained using various methods.

Figure captions

1. DMC energy of the all-electron Ne atom and the pseudo-Ne atom as a function of the time step. The pseudo-Ne results are offset so that the zero-time-step energy matches the all-electron energy. The statistical error bars are smaller than the symbols. “GF mods” refers to the modifications to the DMC Green’s function proposed in Ref. [13]. The “exact” nonrelativistic infinite nuclear mass result is taken from Ref. [3].
2. The same as Fig. 1, but for a Ne^+ ion.
3. IP of all-electron and pseudo Ne as a function of the time step. “GF mods” refers to the modifications to the DMC Green’s function proposed in Ref. [13]. The experimental result is taken from Ref. [2], and the exact nonrelativistic IP is from Ref. [3]. The statistical error bars are smaller than the symbols.

Figure 1

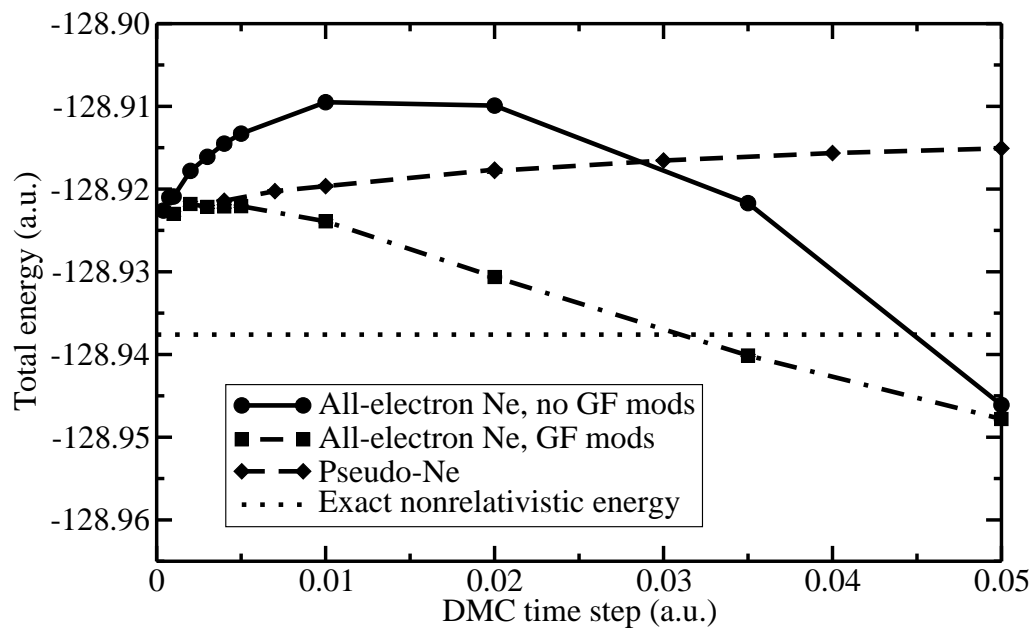


Figure 2

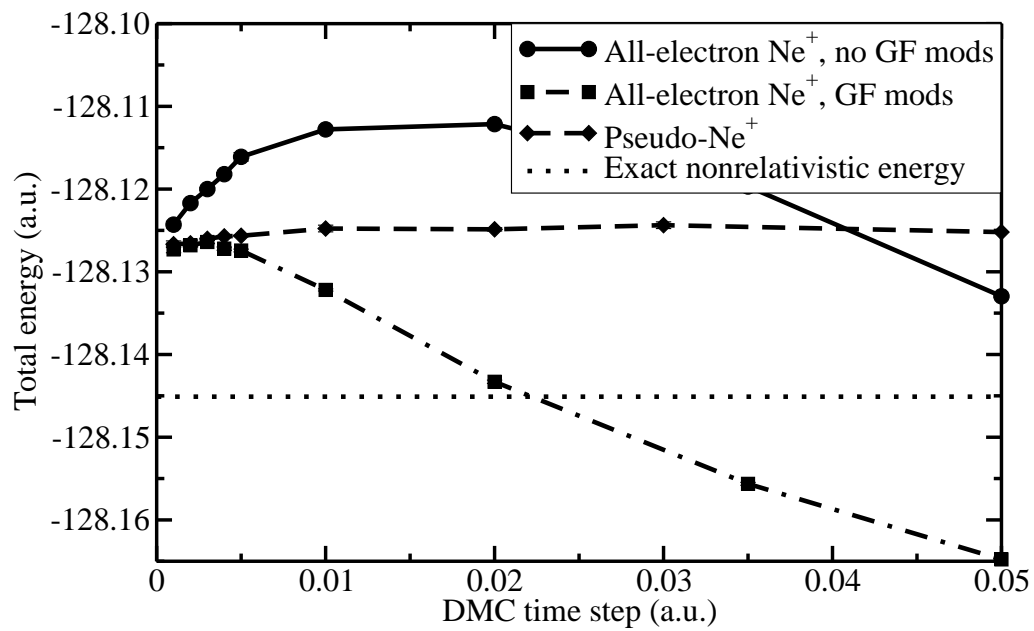


Figure 3

